Creation of Surface Nanostructures in Lanthanum Fluoride Single Crystals by Irradiation with Slow Highly Charged Ions

El-Said, A. S.; Wilhelm, R. A.; Heller, R.; Facsko, S.;

Originally published:

December 2019

Nuclear Instruments and Methods in Physics Research B 460(2019), 137-140

DOI: https://doi.org/10.1016/j.nimb.2019.01.007

*Manuscript

Creation of Surface Nanostructures in Lanthanum Fluoride Single Crystals by Irradiation with Slow Highly Charged Ions

A.S. El-Said[1], R.A. Wilhelm[2,3], R. Heller[2], S. Facsko[2]

[1]Physics Department, King Fahd University of Petroleum and Minerals, Dhahran 31261, Saudi Arabia

[2] Institute of Ion Beam Physics and Materials Research, Helmholtz-Zentrum Dresden-Rossendorf, 01328 Dresden, Germany

[3]Institute of Applied Physics, TU Wien, 1040 Vienna, Austria

Abstract

Slow highly charged ions (HCI) were utilized successfully for the formation of various nanostructures in the surfaces of different materials. The creation mechanism of HCI-induced nanostructures was intensively studied in alkali- and alkaline-earth fluorides. Here, we are investigating another type of fluorine-containing ionic crystals of different crystalline and electronic structure, namely lanthanum fluoride, LaF_3. The single crystals were irradiated with slow (eV-keV) highly charged xenon ions from an Electron Beam Ion Trap Source. After irradiation, the crystals surfaces were investigated by scanning force microscopy. The measured topographic images show nanohillocks emerging from the surface. These nanostructures were observed only after exceeding a well-defined threshold in the potential energy. The role of ion parameters for nanohillocks formation as well as a comparison with results for swift heavy ion irradiations of LaF_3 single crystals are presented. Furthermore, the similarities and differences between LaF_3 and other ionic fluoride crystals, in the creation of surface nanostructures, are discussed.

* corresponding author
e-mail: elsaid@kfupm.edu.sa
Physics Department, King Fahd University of Petroleum and Minerals, Dhahran 31261, Saudi Arabia

1. INTRODUCTION

One of the most important applications of ion beam technology is the fabrication of surface nanostructures in different materials without further treatments, which could cause unwanted modifications. Over many years, swift heavy ions (SHI) of MeV-GeV kinetic energy have been used efficiently and effectively in the creation of various types of nanostructures by single ion impact on a large variety of solid materials [1-4]. During the past few years, slow (eV-keV) highly charged ions (HCI) were used successfully for the creation of similar types of surface nanostructures, i.e. hillocks, caldera-like, craters, and pits, in different materials with an advantage of tailoring only the topmost atomic layers, which is required in various nanoelectronic applications [5-8]. The SHI-induced nanostructures are mainly correlated to the deposition of high electronic energy loss in a localized region along the ion penetration depth, producing strong electronic excitations and ionization in the electronic sub-system. The induced electrons are subsequently coupled to the lattice heating it up, and finally producing the observed nanostructures. In a similar way HCI-induced nanostructures are created [9]. However, the potential energy carried by HCI is considered as the main driving force for the localized electronic excitations and the subsequent electron-phonon coupling.

Ionic fluoride single crystals (e.g., LiF, CaF_2, and BaF_2) are considered as the most intensively studied materials regarding surface nanostructuring using HCI [10-12]. In order to reach a broader understanding of the mechanisms responsible for the creation of nanostructures in this category of materials, comparison with other solids with different properties is required. Therefore, we selected lanthanum fluoride (LaF_3) single crystals to complement the recent studies concerning HCI-induced nanostructures in alkali- and

alkaline-earth fluorides [13,14]. In addition, comparing the response of LaF_3 to HCI with the one for SHI irradiations [15] can highly corroborate the current understanding of the underlying mechanism for nanostructures formation. On the other hand, from the application point of view, LaF_3 is a well-known as an efficient and fast scintillator material with an advantage of the absence of color centers at room temperature [16]. The doping of this material by rare-earth trivalent ions made it an ideally efficient UV laser material [17]. The doped rare-earth 4f electrons are well isolated from the electric fields by the host crystal at the position of the dopant ion. Therefore, extremely sharp lines of the spectra were obtained due to the involved electronic excitations within the 4f configuration [18,19]. These effects are of high importance for using the doped LaF_3 nanoparticles in radiation dosimetry [20].

2. EXPERIMENTAL

The samples in this work are epitaxial (epi)-polished LaF_3 single crystals (from MTI corporation, USA) of size 10 mm x 10 mm x 0.5 mm. The crystals have been grown from the melt in an inert atmosphere along the < 0001 > direction. The substrates were irradiated in a UHV chamber (pressure $\sim 1 \times 10^{-8}$ mbar) at room temperature, and under normal incidence, with highly charged $^{129}Xe^{Q+}$ ions of various charge states from Q=26 to Q=40. The ions were extracted from the Dresden-EBIT (electron beam ion trap) at the Ion Beam Center of HZDR. The ions were extracted in pulsed mode at 4.4 kV. However, for keeping the same kinetic energy (114.4 keV of undecelerated Xe^{26+} ions) for all ions, a two-stage deceleration system was used to slow down the ions of higher charge states (Q > 26+). The utilized ion fluences on the irradiated surface were in the range of 1–5 x 10^9 ions/cm^2. The polished side of the substrate was homogeneously irradiated by

wobbling the sample holder during the elapsed time of irradiation. The parameters of the HCI are listed in Table 1 (SRIM 2010 was used to estimate some of the parameters [21]). After irradiation, the surfaces of LaF_3 substrates were inspected using a Nanoscope III (Bruker) scanning force microscope (SFM). The microscope was operated in contact mode at a constant loading force under ambient conditions. The measurements were performed using non-conductive Si_3N_4 sensors (Veeco Instruments) with triangular cantilevers of force constant ~ 0.1 N/m. The image processing and analysis of SFM topographic images were performed using Nanotec Electronica SL WSxM software (version 5.0 Develop 6.4) [22].

3. RESULTS AND DISCUSSION

SFM measurements were performed on the polished side of LaF_3 single crystals after irradiation with 114.4 keV Xe^{Q+} (Q= 26, 28, 30, 32, 34, 36, 38 and 40). Both the topographic and the simultaneously measured lateral-force images did not show any surface nanostructures after irradiation with Xe^{Q+} ions carrying charges from Q= 26 to Q=34, as shown in Fig.1(a and d). However, surface nanohillock were observed after the exposure to highly charged Xe^{Q+} ($Q \geq 36$) ions, as shown in Fig.1(b, c, e and f) and Fig.2 (a and b). In all cases, the number of the observed hillocks in each image is in fair agreement with the applied ion fluence. The width and height of the hillocks were estimated using line profile across each hillock (see Fig. 2 (c)). Fig.3 shows the frequency distribution of both the width (left) and height (right) for the hillocks created by Xe^{36+}, Xe^{38+} and Xe^{40+} ions. It is observed that the histograms are shifted to higher values for the hillocks induced by higher charge states. The mean values of both the width and height of the created hillocks are shown in Table. 1. Both values increase by

increasing the potential energy, $E_{p,}$, from 27.8 keV to 38 keV. Assuming that this increase is linear, we can estimate ~ 1 nm/keV increase in width and ~ 0.1 nm/keV in height. This is taken into consideration that a threshold of 23.3 keV<$E_p \leq$ 27.8 keV is required for the creation of nanohillocks in LaF_3 single crystals. In comparison to other investigated ionic fluoride crystals, this value is higher than the one (12.0 keV< $E_p \leq$ 15.2 keV) observed for CaF_2 single crystals after irradiation with 10 x q keV HCI, and consequently also higher than the slightly smaller value (8.9 keV< $E_p \leq$ 12.0 keV) by using slower HCI of 150 x q eV kinetic energy [23]. This decrease of potential energy threshold by reducing the kinetic energy of HCI was also confirmed for BaF_2, where the HCI-induced hillocks appeared only by decelerating the highly charged xenon ions to kinetic energy of 15 keV [24]. It should be mentioned that nanohillocks were observed for LaF_3 after irradiation with SHI after exceeding a threshold of electronic energy loss $(dE/dx)_e$ ~ 5 keV/nm [15, 25], which is higher than both $(dE/dx)_e$ and nuclear energy loss $(dE/dx)_n$ for the used 114.4 keV highly charged Xe ions, as shown in Table 1. Therefore, it is obvious from this result as well as: (i) the existence of potential energy threshold for the creation of hillocks, and (ii) the dependence of the hillock size on the used ion potential energy, that the hillocks formation and their size control depend on the deposited potential energy in LaF_3 surface.

The importance of the potential energy was demonstrated in various HCI-nanostructured surfaces [26,27]. Recently it was observed that even for the same material the shape of the obtained HCI-induced nanostructures can additionally be changed by varying the potential energy. This finding was observed in one of the alkali fluorides, namely lithium fluoride single crystals, by creating three different kinds of nanostructures (craters,

caldera-like and hillocks) by simply increasing the charge state and consequently the potential energy of the utilized HCI [14]. The mechanism for the hillocks created by both SHI and HCI in the studied ionic fluorides was described in details using the inelastic thermal spike model [27]. Within this approach, the HCI- and SHI-induced electronic excitations are followed by electron-phonon coupling, which heats the solid lattice. The hillock creation is explained by the rapid quenching of the molten volume created by the deposited energy (kinetic for SHI and potential for HCI). The performed calculation based on the potential energy deposition by HCI in CaF_2 and LiF showed that the molten phase is reached at a threshold potential energy, which is in fair agreement with the observed threshold of hillocks and rim formation [25, 26]. Therefore, we may ascribe the higher potential energy threshold in LaF_3 in comparison to CaF_2 and LiF to the higher melting point. Moreover, the fact that LaF_3 has a tysonite-type trigonal crystalline structure may affect its sensitivity for defects creation. This is demonstrated by the absence of colour centers at room temperature. Only at low temperature ($T \leq 70$ K), self-trapped holes (V_k centers) in the fluorine sub lattice of LaF_3 are observed [16]. It should be noted that in addition to the formation of nanostructures, HCI can also lead to what is termed potential sputtering (sputtering due to potential energy deposition) which may slightly reduce the height of the observed hillocks [29]. This is similar to electronic sputtering, which is induced by the electronic energy loss of SHI [30]. It is further worthwhile mentioning that SHI-induced out-of-plane swelling was observed in LaF_3 and other fluorides, e.g. LiF, CaF_2, BaF_2, and MgF_2 [31]. Despite the fact that all these ionic fluoride crystals have almost similar sensitivity for hillocks creation, they exhibit different responses to SHI-induced swelling, which may indicate that different

mechanisms are involved in both effects. In case of HCI, out-of plane swelling is negligible due to the extremely small penetration depth.

4. Conclusions

Surface nanohillocks were created in LaF_3 single crystals by irradiation with slow highly charged ions. The hillocks were only observed after irradiation with 114 keV Xe^{Q+} ions for Q>36+, implying a potential energy threshold between 23.3 keV and 27.8 keV. The size of the hillocks increases with the potential energy at constant impact kinetic energy. The size of the hillocks produced by 114 keV Xe^{40+} is comparable to the one produced by 540 MeV Xe ions, evidencing the potential energy deposition as the main driving force for surface nanostructuring by HCI. The similarity between SHI and HCI in producing structures of the same shape and almost the same size, not only in LaF_3 but also in other ionic fluorides, may originate from the fact that both of them are depositing their energy initially in the electronic subsystem which is subsequently heating up the phononic subsystem.

Acknowledgments

A.S. E. would like to acknowledge the support by KFUPM (Project No. RG161004).

References

[1] R. Neumann, Nucl. Instr. and Meth. B **151**, 42 (1999).

[2] C. Müller, M. Cranney, A. El-Said, N. Ishikawa, A. Iwase, M. Lang, R. Neumann, Nucl. Instr. and Meth. B **191**, 246 (2002).

[3] O. Ochedowski, O. Osmani, M. Schade, B. K. Bussmann, B. Ban-d'Etat, H. Lebius, and M. Schleberger, Nat. Comm. **5**, 3913 (2014).

[4] H Amekura, H Shinotsuka, H Yoshikawa, Nanotechnology. **28,** 495712 (2017)

[5] M. Tona, Y. Fujita, C. Yamada, S. Ohtani, Phys. Rev. **B 77**, 155427 (2008).

[6] A.S. El-Said, R.A. Wilhelm, R. Heller, and S. Facsko, C. Lemell, G. Wachter, J. Burgduorfer, R. Ritter and F. Aumayr, Phys. Rev. Lett. **109**, 117602 (2012).

[7] R. Ritter, R. A. Wilhelm, R. Ginzel, G. Kowarik, R. Heller, A.S. El-Said, R. M. Papaleo, W. Rupp, J. R. Crespo L´opez-Urrutia, J. Ullrich, S. Facsko, F. Aumayr, EPL **97**, 13001 (2012).

[8] Richard A. Wilhelm, Ayman S. El-Said, Franciszek Krok, Rene Heller, Elisabeth Gruber, Friedrich Aumayr, Stefan Facsko, Prog. Surf. Sci. **90**, 377 (2015).

[9] F. Aumayr, A.S. El-Said, and W. Meissl, Nucl. Instr. and Meth. B **266**, 2729 (2008).

[10] A.S. El-Said, W. Meissl, M.C. Simon, J.R. Crespo Lopez-Urrutia, I.C. Gebeshuber, J. Laimer, HP. Winter, J. Ullrich, and F. Aumayr, Radiat. Eff. Defect Solids **162** (2007).

[11] A.S. El-Said, W. Meissl, M. Simon, J.R. Crespo López-Urrutia, I.C. Gebeshuber, HP. Winter, M. Lang, F. Aumayr, Nucl. Instr. and Meth. B **256**, 364 (2007).

[12] A.S. El-Said, R. Heller, F. Aumayr, S. Facsko, Phys. Rev. **B 82**, 057027 (2010).

[13] M. Karlušić, C. Ghica, R.F. Negrea, Z. Siketić, M. Jakšić, M. Schleberger, S. Fazinić, New J. Phys. **19**, 023023 (2017).

[14] A.S. El-Said, R. A. Wilhelm, R. Heller, M. Sorokin, S. Facsko, F. Aumayr, Phys. Rev. Lett. **117**, 126101 (2016).

[15] A.S. El-Said, R. Neumann, K. Schwartz, C. Trautmann, Surf. and Coat. Technol. **158**, 522 (2002).

[16] E.d. Thoma, H. Shields, Y. Zhang, B.C. McCollum, R.T. Williams, J. Lumin. **71**, 93 (1997).

[17] A.S Oreshonkov, E M Roginskii, A.S Krylov, A.A Ershov, V.N Voronov, J. of Phys. Cond. Matt. **30**, 255901 (2018).

[18] .J. Wojtowicz, M. Balcerzyk, E. Berman, A. Lempicki, Phys. Rev. B **49**, 14880 (1994).

[19] M. Dagenais, M. Downer, R. Neumann, N. Bloembergen, Phys. Rev. Lett. **46**, 561 (1981).

[20] Y. Liu, W. Chen, S. Wang1, A, G,. Joly, S, Westcott, B, Kuan Woo, J. Appl. Phys. **103**, 063105 (2008).

[21] J.F. Ziegler, M.D. Ziegler, J. P. Biersack, Nucl. Instr. and Meth. B **268**, 1818 (2010).

[22] I. Horcas et al., Rev. Sci. Instr. **78**, 013705 (2007).

[23] A.S. El-Said, R. Heller, W. Meissl, R. Ritter, S. Facsko, C. Lemell, B. Solleder, I. Gebeshuber, G. Betz, M. Toulemonde, W. Möller, J. Burgdörfer, F. Aumayr, Phys. Rev. Lett. **100**, 237601 (2008).

[24] A.S. El-Said, R. Heller, S. Facsko, Nucl. Instr. and Meth. B **269**, 901 (2011).

[25] A.S. El-Said, F. Aumayr, S. Della-Negra , R. Neumann, K. Schwartz, M. Toulemonde, C. Trautmann, K.-O. Voss, Nucl. Instr. and Meth. B **256**, 313 (2007).

[26] R. Heller, S. Facsko, R. A. Wilhelm, W. Möller, Phys. Rev. Lett. **101**, 096102 (2008).

[27] S. Facsko, R. Heller, A.S. El-Said, W. Meissl, F. Aumayr, Phys. Cond. Mat. **2**, 224012 (2009).

[28] M. Toulemonde, C. Dufoure, A. Meftah, E. Paumier, Nucl. Instr. and Meth. B 166-167**,** 903 (2000).

[29] F. Aumayr, H. Winter, Phil. Trans. R. Soc. A **362,** 77 (2004).

[30] M. Toulemonde, W. Assmann, C. Trautmann, F. Grüner, Phys. Rev. Lett. **88**, 057602 (2002).

[31] A.S. El-Said, M. Cranney, N. Ishikawa, A. Iwase, R. Neumann, K. Schwartz, M. Toulemonde, C. Trautmann, Nucl. Instr. and Meth. B **218**, 492 (2004).

TABLE 1. *Parameters of the used ions for irradiation of LaF_3 (potential energy E_{pot}, kinetic energy E_{kin}, electronic stopping $(dE/dx)_e$, nuclear stopping $(dE/dx)_n$, and mean range R calculated using SRIM [21]) and the nanohillocks dimensions (mean diameter D and mean height H).*

Ions	E_{pot} (keV)	E_{kin} (keV)	$(dE/dx)_e$ (keV/nm)	$(dE/dx)_n$ (keV/nm)	*R* (nm)	*D* (nm)	*H* (nm)
Xe^{26+}	8.9 keV	114.4	0.4	3.1	32.5	--	--
Xe^{28+}	12.0 keV	114.4	0.4	3.1	32.5	--	--
Xe^{30+}	15.4 keV	114.4	0.4	3.1	32.5	--	--
Xe^{32+}	19.1 keV	114.4	0.4	3.1	32.5	--	--
Xe^{34+}	23.3 keV	114.4	0.4	3.1	32.5	--	--
Xe^{36+}	27.8 keV	114.4	0.4	3.1	32.5	20.5 ± 2.0	0.6 ± 0.3
Xe^{38+}	33.0 keV	114.4	0.4	3.1	32.5	22.6 ± 2.5	0.8 ± 0.2
Xe^{40+}	38.0 keV	114.4	0.4	3.1	32.5	24.5 ± 2.5	1.1 ± 0.3

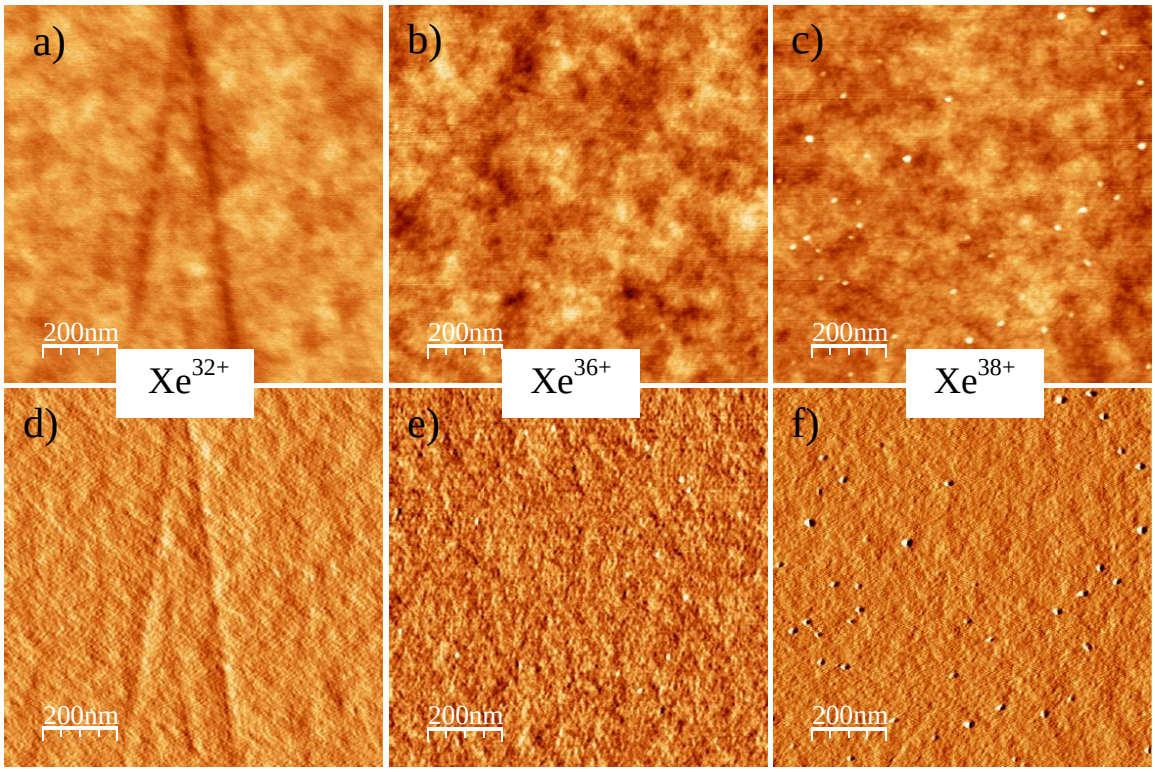

Fig. 1. SFM topographic (a, b and c) and lateral force (d, e and f) images of a LaF_3 single crystals irradiated with 114.4 keV Xe^{32+}, Xe^{36+}, and Xe^{38+} ions.

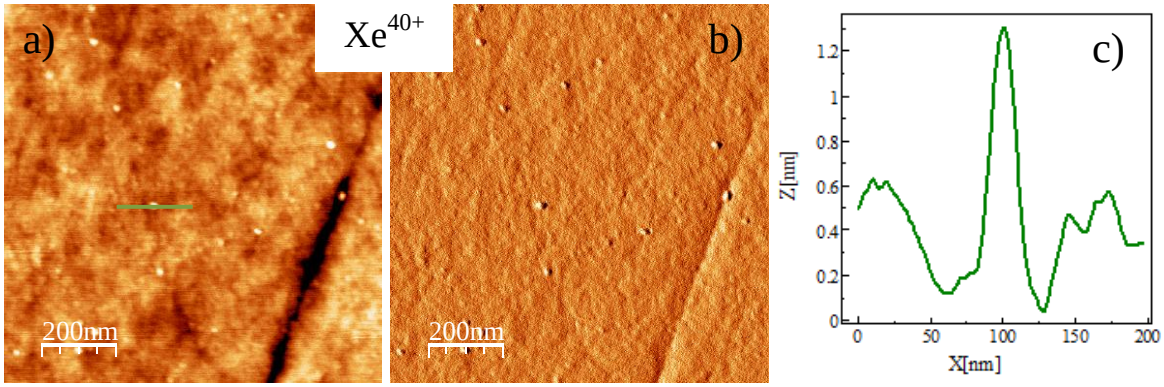

Fig. 2. SFM topographic (a) and lateral force (b) images of LaF_3 single crystals irradiated with 114.4 keV Xe^{40+} ions. Representative line profile (c) of a hillock is shown.

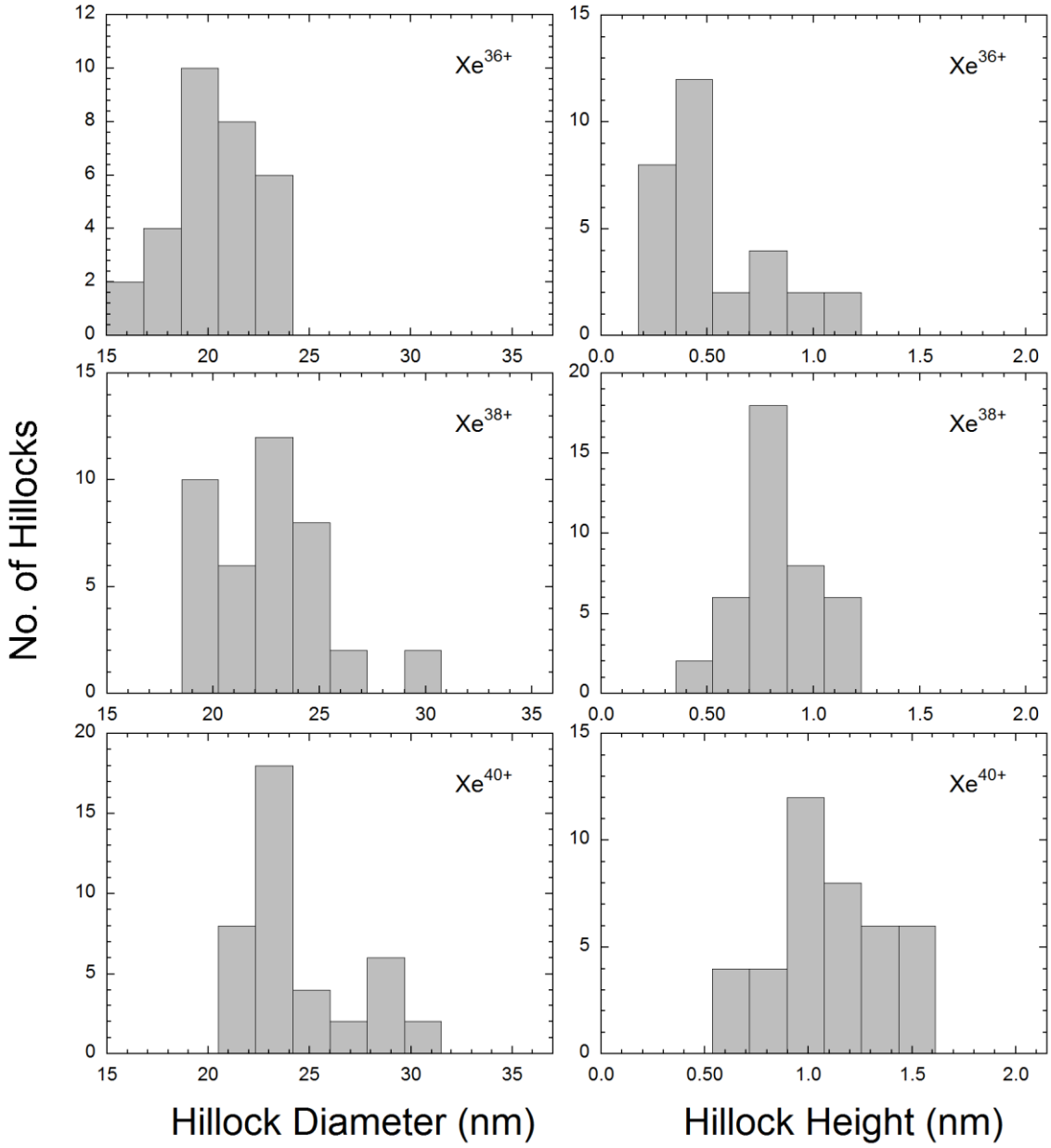

Fig. 3. Statistical distribution of hillock diameter (left) and hillock height (right) for LaF_3 surfaces irradiated with 114.4 keV Xe^{36+}, Xe^{38+}, and Xe^{40+} ions.

Table (already exist in body of manuscript)

TABLE 1. *Parameters of the used ions for irradiation of LaF_3 (potential energy E_{pot}, kinetic energy E_{kin}, electronic stopping $(dE/dx)_e$, nuclear stopping $(dE/dx)_n$, and mean range R calculated using SRIM [21]) and the nanohillocks dimensions (mean diameter D and mean height H).*

Ions	E_{pot} (keV)	E_{kin} (keV)	$(dE/dx)_e$ (keV/nm)	$(dE/dx)_n$ (keV/nm)	*R* (nm)	*D* (nm)	*H* (nm)
Xe^{26+}	8.9 keV	114.4	0.4	3.1	32.5	--	--
Xe^{28+}	12.0 keV	114.4	0.4	3.1	32.5	--	--
Xe^{30+}	15.4 keV	114.4	0.4	3.1	32.5	--	--
Xe^{32+}	19.1 keV	114.4	0.4	3.1	32.5	--	--
Xe^{34+}	23.3 keV	114.4	0.4	3.1	32.5	--	--
Xe^{36+}	27.8 keV	114.4	0.4	3.1	32.5	20.5 ± 2.0	0.6 ± 0.3
Xe^{38+}	33.0 keV	114.4	0.4	3.1	32.5	22.6 ± 2.5	0.8 ± 0.2
Xe^{40+}	38.0 keV	114.4	0.4	3.1	32.5	24.5 ± 2.5	1.1 ± 0.3

Figure 1
Click here to download high resolution image

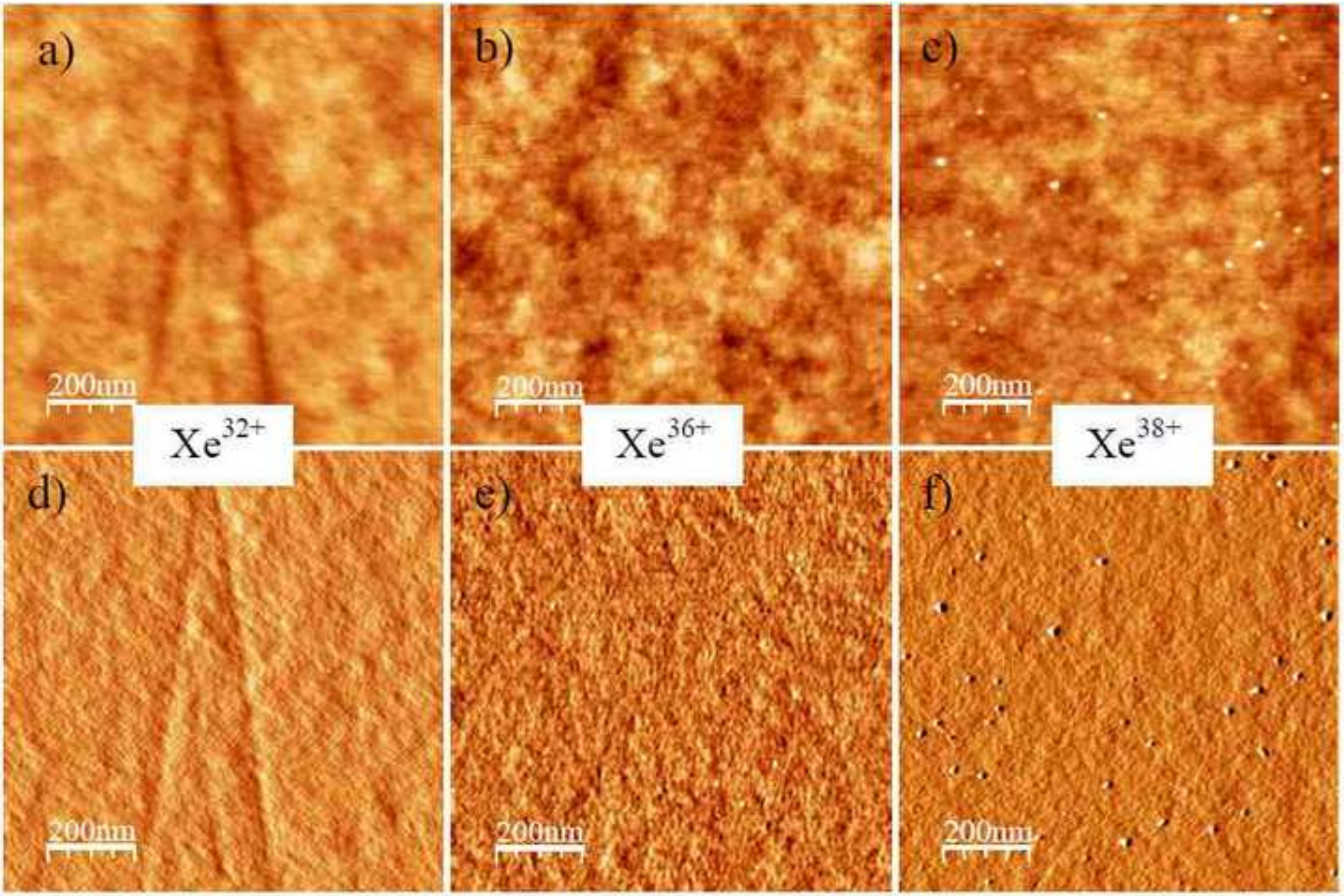

Figure 2
Click here to download high resolution image

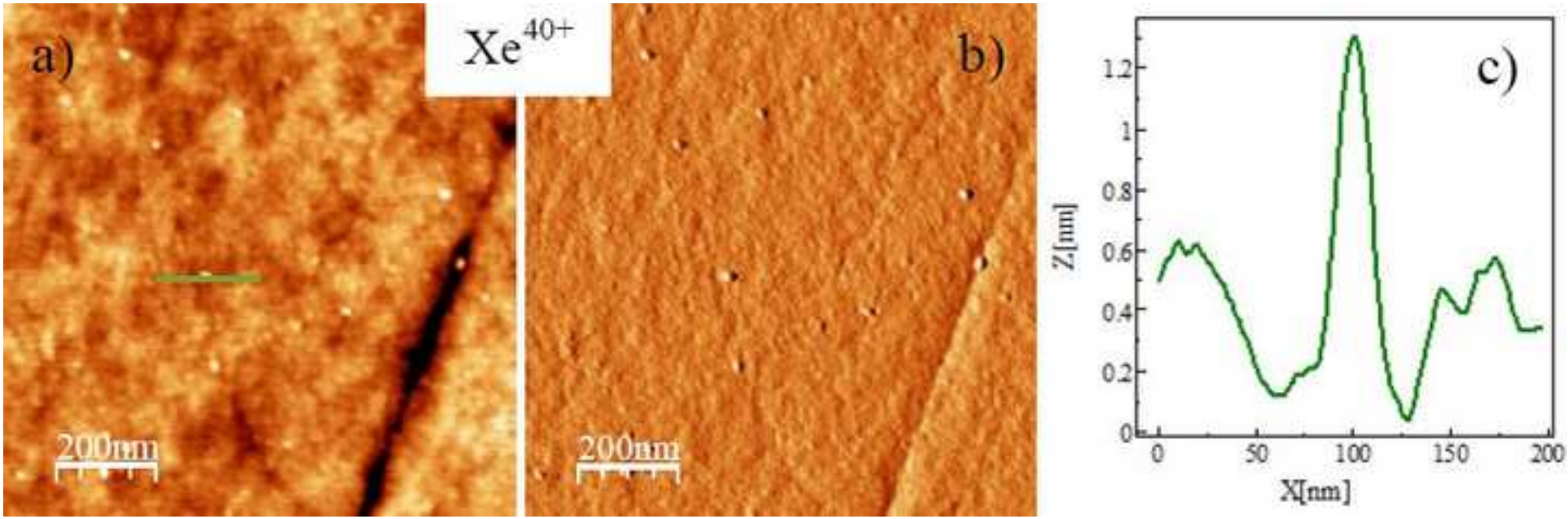

Figure 3
Click here to download high resolution image